Origin and multiple crystallization of the kamafugite-carbonatite association: the San Venanzo-Pian di Celle occurrence (Umbria, Italy)

F. Stoppa

Dipartimento di Scienze della Terra, Università di Perugia, Perugia, Italy

AND

A. Cundari

Dipartimento di Geofisica e Vulcanologia, Università Federico II, Napoli, Italy

ABSTRACT

The Late Pleistocene kamafugite−carbonatite association at San Venanzo-Pian di Celle forms part of the Umbria-Latium Ultra-alkaline District (ULUD) of central Italy and, together with Toro-Ankole, SW Uganda and Mata de Corda, Brazil, represents one of three similar occurrences so far reported worldwide.

Excellent field exposure and stratigraphic control prompted a study of the kamafugite−carbonatite suite and related phase interactions to understand the nature of the distinct mineral assemblages of the pyroclasts, compared to that of the lavas, the former containing essential potassium feldspar and aluminous diopside crystals, absent in the latter.

The pyroclastic rocks represent a small amount of magma characterized by ubiquitous mantle xenocrysts and emplaced by early high-velocity eruptions. All the investigated specimens show a high $Mg/(Mg+Fe^{2+})$ ratio (0.84−0.93) and high compatible elements (Ni+Cr>1000 ppm). Lavas (venanzite, i.e. leucite melilitite) and a sill (uncompahgrite, i.e. melilitolite) represent final events in the volcanic sequence. They yielded a (Na+K)/Al ratio of *c*. 1.1 and are larnite-bearing in the CIPW norm. Glass from the lapilli is peralkaline, i.e. (Na+K)/Al>2, and close to the lava in composition. Glass from melilitolite yielded CIPW Or and Hy and is strongly peralkaline, i.e. (Na+K)/Al = 5−6. The lapilli typically exhibit concentrically zoned structures which compound subliquidus venanzite phases, e.g. melilite, leucite, and kalsilite, with mantle xenolithic/xenocrystic debris and carbonatite phases. These lapilli represent a distinct variant of the venanzite liquid, mechanically fractionated and quenched by the diatremic process.

Mantle-normalized HFSE for both lava and lapilli show typical extrusive-carbonatite patterns. Carbonatitic beds intercalated with the pyroclastic suite are distinct and typically consist of carbonates high in Sr, Ba and *REE*. Primary carbonate yielded C isotope compositions ranging from −5.0 to −6.0 $\delta^{13}C$‰, falling within the range of mantle compositions. Distinct differentiation trends of the venanzite magma and its derivatives were recognized, hinging on the coexistence of the silicate and carbonatite fractions. Potential sanidine crystallization trends are suggested, distinct from the venanzite→melilitolite trend, reported for Oldoinyo Lengai assemblages.

Unusual aspects of the San Venanzo rock association, relative to similar rock types elsewhere, include the combination of a rare mantle source composition with a lithosphere about 80 km thick. A genetic model for the origin of the San Venanzo kamafugite−carbonatite association and related carbonate-silicate interactions is proposed and discussed. This may be relevant to the petrogenesis of similar rocks elsewhere, particularly in the light of the detailed data on the pyroclasts.

KEYWORDS: multiple crystallization, kamafugite−carbonatite, pyroclastic, xenolith, mantle-source.

Introduction

THE kamafugite—carbonatite association involves the rarest igneous rock types, typically confined to continental environments and related to extensional tectonics, e.g. Toro and Ankole, SW Uganda (Bell and Powell, 1969), Mata da Corda, Minas Gerais, Brazil (de Albuquerque Sgarbi *et al.*, 1993) and Umbria-Latium Ultra-alkaline District, ULUD, central Italy, Fig.1, (Stoppa and Lavecchia, 1992).

The mantle source for this association may be assumed to be a peridotite in equilibrium with carbonatite melt (Dalton and Wood, 1993) and special conditions for magma genesis and ascent to the surface would be involved (Bailey, 1985, 1990; LeBas, 1987). Also, the kamafugite—carbonatite system implies unusual and perhaps unique physico-chemical processes of elemental partitioning between carbonatite and silicate components (Stoppa and Cundari, 1995). These are not necessarily confined to the mantle source region and may extend to the magma entrainment and explosive propagation through the lithosphere (Bailey, 1985). Ubiquitous mantle xenoliths/ xenocrysts suggest a direct and rapid ascent of the carbonatitic liquid from the mantle source (Bailey, 1993). However, deep-seated fluidification may have substantially modified, at least mechanically, the (C,H)-bearing mantle melts, with partial to complete separation of the initial, i.e. 'primary', carbonatite from the cognate silicate liquid.

Since earlier investigations of ULUD San Venanzo lava (e.g. Gallo *et al.*, 1984; Cundari and Ferguson, 1991), important information has emerged from a detailed mineralogical and petrochemical study of the associated pyroclastic rocks, pointing to a distinct crystallization history relative to that of the lava.

This paper documents the occurrence and some fundamental petrological aspects of typical ULUD pyroclastic rocks, compared with the related lava. An interpretation of their genetic relationships is offered, based on the excellent stratigraphy exposed at San Venanzo—Pian di Celle, which may be useful where crucial field data are not available.
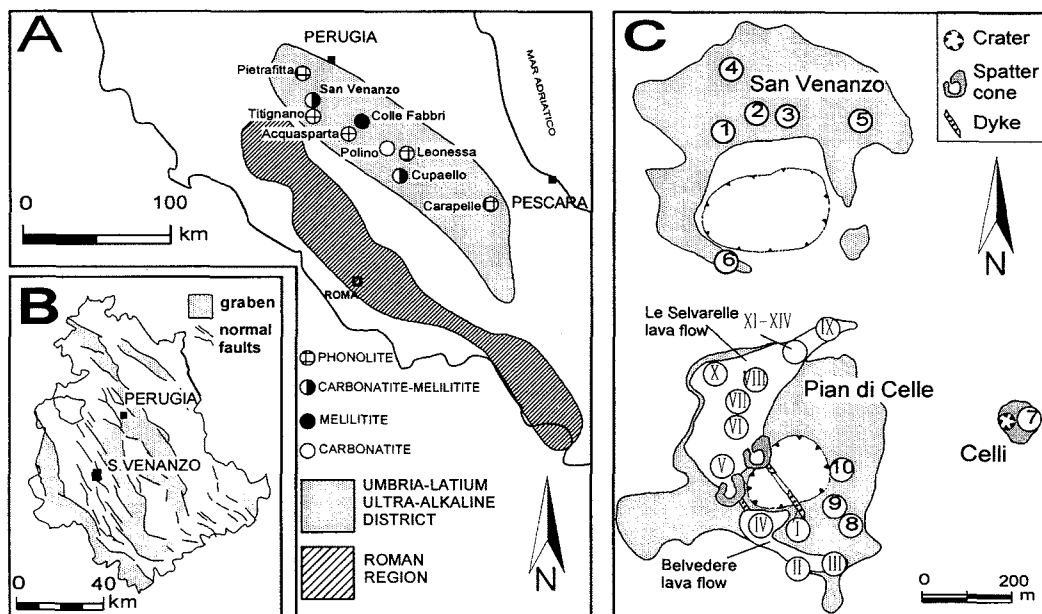

FIG. 1A. Sketch map of the Umbria-Latium Ultra-alkaline District (ULUD) and adjacent Roman Region. B. Detailed location of San Venanzo and related structural geology. C. Geological sketch map of the San Venanzo formations and sampling sites.

Geological notes and rock types

The post-Pleistocene volcanoes of San Venanzo and Pian di Celle (Fig. 1) are located on the western margin of a graben forming the Tiber valley (Fig. 1B), and represents the most prominent among several ULUD volcanic centers (Fig. 1A). The dominant structures vary from normal to normal-oblique faults striking N–S to NW–SE and conforming with the regional trends of the Tiber graben (Fig. 1B). Extensional tectonics dominated this province since the Pliocene (Lavecchia et al., 1994).

The volcanic materials are associated with maar-type vents, and formed mainly tuffs and lapilli with subordinate lava, dykes and a sill. The lava is represented by two flows, Le Selvarelle and Belvedere, which originated from three distinct vents marked by spatter cones and located on a NNW–SSE trending fracture zone, west of the main Pian di Celle crater (Fig. 1C). The sill is c. 1m thick and overlies the sedimentary basement at the northeastern tip of the Le Selvarelle flow (Fig. 1C). Above the sill, the lava is brecciated and penetrated by pegmatoid dykelets from the sill. These dykelets show sharp, chilled contacts and a coarse-grained facies in the middle sections, grading to fine-grained toward the contacts with the lava.

The total surface area covered by these rocks is c. ⅓ km^2, corresponding to c. 7×10^6 m^3, nearly 90% of which are pyroclastic rocks. A detailed geological map of the area, lithology, stratigraphy and related volcanic activity are given in Stoppa and Sforna (1995) and Stoppa (1996).

San Venanzo

The San Venanzo suite is formed, from stratigraphic top to bottom, by three pyroclastic facies, i.e. a lithic tuff, a lapilli tuff and a lithic breccia. The igneous components of the lithic breccia are dominated by highly vesiculated glassy lapilli and coarse-grained ash. Green-grey euhedral to subhedral forsterite and light to dark green subhedral diopside crystals, 2–3 mm along the c-axis, are abundant in the finer-grained layers and lowermost 2 m of the deposit. Potassium feldspar crystals 3–4 mm along the c-axis are common in the matrix and abundant in crystal-rich layers. In addition to highly vesiculated lapilli and coarse-grained ash, the lapilli tuff contains microvesiculated carbonatitic bombs and lithics in a fine-grained calcite matrix. The lapilli contain phenocrystal/xenocrystal forsterite with chromite and calcite inclusions in a matrix of abundant amoeboid calcite, subordinate leucite, spinels, melilite and glass. The juvenile component of the lithic tuff is mainly composed of small vesiculated lapilli and coarse ash. Accessory lithics are generally angular and multi-coloured marl fragments which make up from 5 wt.% to 50 wt.% of the whole rock. Crystal-rich layers occur and mainly consist of varying proportions of euhedral forsterite, light and dark green diopside and alkali-feldspar. Crystals are mantled by a selvedge of glassy groundmass.

Pian di Celle

The Pian di Celle suite consists, from stratigraphic top to bottom, of a lava, intruded by a sill, a scoria tuff, a chaotic breccia and a lapilli ash-tuff. The crystal component of the lapilli ash-tuff is mainly discrete euhedra and glass-mantled crystals of forsterite and diopside. Carbonatite ash layers 2–3 cm thick occur. The chaotic breccia, composed mainly of vesicular carbonatite, melilitite lapilli and bombs, forms the dominant part of the sequence. Lapilli typically consist of near-spherical, concentric shells around lithic fragments and dunite microliths. A typical carbonatite assemblage consisting of calcite, apatite, perovskite and magnetite alternates with shells containing phenocrystal forsterite, melilite, kalsilite and leucite in a glassy matrix, first noted by Mittempergher (1965). The lapilli are supported by a very fine and compact carbonatite containing glass shards, forsteritic olivine and light to dark green, subhedral pyroxene, similar to that in the San Venanzo suite. The scoria tuff is formed by large lapilli and lava bombs locally aggregated in rheomorphic flows.

The Pian di Celle lava was originally called euktolith by Rosenbusch (1898) and venanzite by Sabatini (1899). It was assigned to the mafurite series from South-West Uganda, madupite from the Leucite Hills, Wyoming by Holmes (1942) and to kamafugites, i.e. group II of Foley et al. (1987), by Sahama (1974). In this paper we retain Sabatini's (1899) terminology, bearing in mind that the rock is an olivine-leucite-kalsilite melilitite according to LeMaitre (1989).

The sill is formed by a coarse-grained, blue-black, dense rock with irregular patches of melilite poikilitically enclosing nepheline prisms and polycrystal inclusions. Leucite forms equant, twinned crystals or is intergrown with Ti-magnetite. Gold-brown phlogopite sheafs and clinopyroxene form variolitic structures in a

finer-grained carbonate groundmass or reaction coronas around melilite and leucite. Olivine, commonly enclosing chromian spinel and poly-crystal inclusions, is strongly corroded and rimmed by phlogopite and monticellite. A typical mode of the sill rock is 28% melilite, 25% leucite, 12% calcite, 9% phlogopite, 7% (nepheline+kalsilite), 5% clinopyroxene, 4% Ti-magnetite-ulvöspinel, 2% apatite, 2% (olivine + monticellite), 3% accessory phases and 3% glass. Based on the modal composition, this rock may be classified as calcite-leucite uncompahgrite, (LeMaitre, 1989). In this paper it is referred to as melilitolite for simplicity.

Celli

Celli is a distinct vent with a radially dipping lapilli-tephra ring, filled with concentrically grown, glassy lapilli and country rock debris.

In summary, the volcanoes of San Venanzo and Pian di Celle opened their activity subcontemporaneously, with multiple explosive events characterized by pyroclastic deposits with typical venanzite mineralogy, but distinct from the latter in containing essential glass. Notably the earliest San Venanzo pyroclasts contain alkali feldspar-rich layers and a carbonatitic tuff matrix with abundant alkali feldspar and green pyroxene, absent from venanzite. The lava and associated melilitolite sill represent the closing events of the San Venanzo-Pian di Celle volcanoes.

The nature of the pyroclasts is heterogeneous down to cm scale due to strong mechanical sorting of crystal, ash and lithic fragments, operated through vigorous volcanic activity. Therefore, only analyses of identifiable juvenale components, i.e. crystals, glass and lapilli are given in this paper. Bulk pyroclast compositions compound also variable ash fractions+xeno-crystal/xenolithic materials and are generalized in some diagrams for comparison.

Mineral and glass chemistry

Mineral and bulk-rock chemistry of venanzite and melilitolite are given in Gallo *et al.* (1984), Peccerillo *et al.* (1988), Cundari and Ferguson (1991) and Stoppa *et al.* (1997). In this section we present the chemistry of individual crystals in tuff matrix and glass from lapilli.

Chemical data of common minerals were obtained by means of CAMECA-SX50 systems at the Department of Earth Sciences, Padova University and The Natural History Museum (Department of Mineralogy), London, using standard procedures. Precision for major and minor elements is better than 5% and generally better than 10%, respectively. Typical compositions and structural formulae are given in Tables 1 to 5. Glass analyses from lapilli are given in Table 6, compared with glass from melilitolite.

Olivine

Representative olivine analyses and structural formulae are given in Table 1. Similar to olivine variations from other ULUD localities, most olivines compositions form a continuous suite, generally falling within the highest forsterite values reported for olivine in mantle xenoliths from kimberlites (Fig. 2A,B). $Mg/(Mg+Fe^{2+})$, Mg#, is consistently high (0.92−0.93). Ca and Mn tend to increase from core to rim, respectively (not shown). Chromite inclusions are common (Table 5; Nos.3−4). Fe-Ni sulphide spherules less than 100 μm across (Table 5; Nos.5−6), possibly pyrite−vaesite solid solutions (Clark and Kullerud, 1959), are similar to those reported in olivine melilitite from Namaqualand (Moore and Erlank, 1985) and kimberlite (Dawson, 1980; Mitchell, 1986, 1995).

In contrast, olivine from melilitolite yielded lower Mg# (0.65), the highest CaO (1.37 wt.%) and MnO (up to 1 wt.%), while intermediate Mg#, CaO and MnO, respectively, were obtained from groundmass olivine from venanzite (Cundari and Ferguson,1991; Table 1; Nos.1−4).

Clinopyroxene

Typical electron microprobe analyses (Nos.1−9; Table 2) indicate that the green clinopyroxene is generally diopside (Morimoto, 1988), compositions with the lowest Ti being Cr-diopside (Cr = 0.03 atoms per formula unit, a.f.u.). This pyroxene is close in composition to pyroxenes from kimberlites (Dawson, 1980). Calculation of the structural formulae on the basis of 6 Oxygens and $(Fe^{2+}+Fe^{3+}) = Fe^{2+}$ generally yielded (M1+M2) = 2.00 ± 0.02, suggesting that the fraction of Fe occurring as Fe^{3+} may not be significant.

Distinct from the pyroxene composition from melilitolite and venanzite, where Al<(2-Si), showing a low Al *vs.* high Ti trend, Al is sufficient to fill the T site to 2.00 a.f.u., showing a high Al *vs.* low Ti trend (Fig. 2C). Mg# is generally higher than 0.88 and correlates with high Cr for Mg#>0.90, while the pyroxene from melilitolite and venanzite generally falls at

TABLE 1. Representative electron microprobe analyses and structural formulae of olivine from San Venanzo (SV) and Pian di Celle (PC) pyroclastic rocks

	1 PC1	2 PC1	3 PC1	4 SV1	5 SV1	6 SV4
SiO_2	41.0	42.3	42.3	41.6	40.5	41.2
Al_2O_3	<0.01	0.04	0.04	<0.01	<0.01	<0.01
Cr_2O_3	0.19	0.07	0.08	0.03	<0.01	<0.01
MgO	49.6	49.0	48.9	50.18	50.6	50.5
CaO	0.20	0.21	0.22	0.47	0.65	0.64
MnO	<0.01	0.10	0.10	0.14	0.16	0.14
FeO	8.38	7.74	7.83	7.11	7.64	7.49
NiO	0.33	0.31	0.30	0.14	<0.01	<0.01
V_2O_3	0.24	0.21	0.25	0.16	<0.01	<0.01
Total	99.94	100.61	100.74	100.10	99.55	99.97

Cations based on 4 Oxygens
Si	1.000	1.020	1.020	1.007	0.990	1.000
Al	0.000	0.001	0.001	0.000	0.000	0.000
Cr	0.004	0.013	0.015	0.006	0.000	0.000
Mg	1.804	1.762	1.757	1.811	1.844	1.828
Ca	0.005	0.005	0.006	0.012	0.017	0.017
Mn	0.000	0.002	0.002	0.003	0.003	0.003
Fe^{2+}	0.171	0.156	0.158	0.144	0.156	0.152
Ni	0.006	0.006	0.006	0.003	0.000	0.000
V	0.010	0.010	0.010	0.003	0.000	0.000
Total	3.00	2.98	2.97	2.99	3.01	3.00
Fo	0.91	0.92	0.92	0.93	0.92	0.92

lower Mg#, Cr (Fig. 2D) and may contain significant Na (e.g. No.10; Table 2). Similar high-Ti, high-Na vs. low-Al trends, respectively, were reported from the pyroxene in a peralkaline pegmatoid differentiate forming veinlets in a leucitite from the New South Wales suite (Cundari and Ferguson, 1982). This supports the view that the pyroxene from the San Venanzo and Pian di Celle pyroclasts is genetically distinct from the pyroxene evolved from the San Venanzo-type lava.

Alkali feldspar

Alkali feldspar is a potassium feldspar with Na_2O up to 2.07 wt.% (22 mol.% albite), BaO up to 3.15 wt.% and SrO up to 2.05 wt.% (Table 3). BaO and SrO are the highest reported in alkali feldspars (Smith and Brown, 1989). These authors noted that "Sr-rich alkali feldspars are characteristically related to regions of alkaline volcanism probably associated with continental rifting...",

and reported comparable Sr and Ba only from nepheline syenites from Greenland and Russian alkaline provinces. They also reported comparable Ba in alkali feldspar from leucitites, lamproites, carbonatites and various ultrapotassic rocks. However, low Fe_2O_3, relative to CaO, and low Na_2O indicate that the San Venanzo feldspar is distinct from that typical of lamproites (Mitchell and Bergman, 1991).

Carbonate

Carbonate (Table 4) is a low-Mg (less than 3 wt.% MgO) calcite with high SrO (up to 1 wt.%) and relatively high BaO and *LREE* (0.07 wt.% and greater than 300 ppm, respectively). These concentrations are typical of calcite from carbonatites (Kapustin, 1980). Higher *LREE* concentrations, up to *c.* 2 wt.%, have been reported by Stoppa and Woolley (1997), although the contribution of unresolved *REE* carbonates may have been significant.
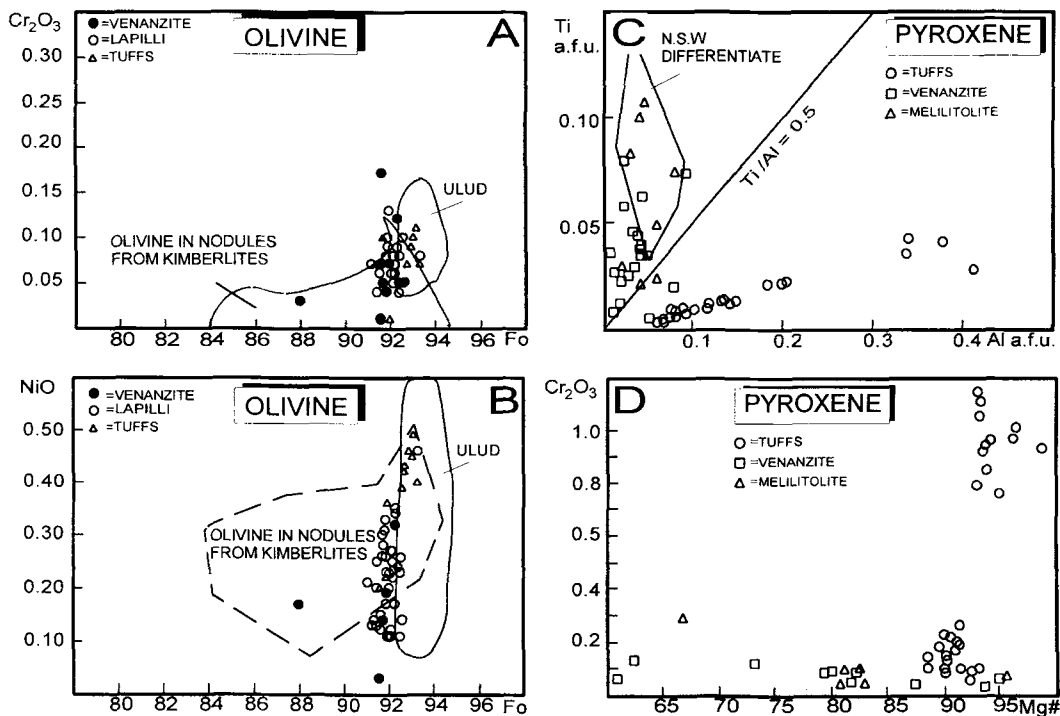
FIG. 2A, B. Compositional variation of San Venanzo olivine in terms of Fo (mol.%) vs. Cr₂O₃ and NiO, respectively (wt.%), compared with olivine composition from other ULUD localities (Stoppa and Lupini, 1993; Brozzetti and Stoppa, 1995) and kimberlites (Dawson, 1980; Mitchell, 1986). C, D. San Venanzo pyroxene variation in terms of Al−Ti (atoms per formula unit, a.f.u.) and 100Mg/(Mg+Fe^{2+})(a.f.u.)-Cr₂O₃ (wt.%), respectively. Generalized field for the pyroxenes from a pegmatoid veinlet in leucitite from the New South Wales leucitite suite is from Cundari and Ferguson, 1982.

Fe-Ti-Cr oxides and sulphides

Remarkably constant in composition throughout the investigated ULUD pyroclastic suite, Fe-Ti-Cr oxides are magnetite and chromite, represented by analyses Nos.1, 2 and Nos.3, 4, respectively in Table 5. Typical Fe-Ni sulphide compositions are represented by analyses Nos.5, 6.

Glass

Oxide totals of glass analyses (Table 6) tend to be significantly low, particularly for the melilitolite groundmass glass. This is largely attributed to undetermined elements, particularly *REE*, B, Li, Zr, F, S and Cl. Despite the determination of F (0.9−1.4 wt.%), Cl (up to 0.5 wt.%) and SO₃ (0.5−1.8 wt.%), low totals (84−91 wt.%) are common also for melt inclusions in olivine from the melilitolite

reported by Stoppa *et al.* (1997). These authors also optically identified salt phases, possibly (K,Na)carbonates, in the glass or bubble inclusions in melilite from the same rock.

Glass from the melilitolite groundmass is strongly peralkaline, i.e. (Na+K)/Al >5, with low Mg#, generally lower than 0.30, compared with glass compositions from lapilli, which are mildly peralkaline (Na+K)/Al>2) with Mg#>0.66. The Fe₂O₃/FeO ratio of the glass analyses was adjusted to 0.5, which is the melilitolite mean analytical value (Table 7, No.12). This differs slightly from 0.8, corresponding to that for venanzite No.11. The CIPW norm, calculated on the basis of Fe₂O₃/FeO = 0.5, shows the presence of Q, Or and Hy in the melilitolite glass, contrasting with the strongly SiO₂-undersaturated, Ol- and Cs-normative compositions of the lapilli glass. It should be noted that these distinctions

278

TABLE 2. Representative electron microprobe analyses and structural formulae of core (c) and rim (r) clinopyroxene from San Venanzo and Pian di Celle pyroclastic rocks. Specimen captions as in Table 1. A typical pyroxene composition from melilitolite (MEL 10) is given for comparison

	1 SVc	2 SVc	3 SVr	4 SVr	5 SVc	6 SVr	7 PC	8 PC	9 PC	10 MEL
SiO_2	53.9	52.9	53.7	52.6	49.2	46.7	54.0	51.1	46.7	52.0
TiO_2	0.19	0.17	0.28	0.37	0.80	1.45	0.34	0.10	1.00	1.73
$Fe2O3$	<0.01	<0.01	<0.01	<0.01	3.14	1.80	<0.01	<0.01	2.41	1.33
Al_2O_3	1.52	1.66	1.84	2.12	4.63	8.60	1.97	6.65	9.45	0.47
Cr_2O_3	0.79	1.05	0.26	0.09	0.10	<0.01	0.23	<0.01	<0.01	<0.01
MgO	17.3	17.1	16.08	15.9	14.7	12.5	16.5	15.7	12.0	10.8
CaO	23.3	23.2	24.2	24.5	24.0	22.1	24.1	21.5	23.9	21.6
MnO	0.12	<0.01	<0.01	0.08	0.12	0.09	0.11	<0.01	<0.01	<0.01
FeO	2.36	2.23	2.70	3.10	1.90	5.76	3.22	4.99	4.65	10.5
Na_2O	0.16	0.18	0.12	0.07	0.12	0.16	0.11	<0.01	<0.01	1.37
Total	99.64	98.49	99.18	98.75	98.38	99.02	100.59	99.99	99.88	99.67
Cations based on 6 Oxygens										
Si	1.964	1.952	1.969	1.945	1.848	1.757	1.957	1.861	1.742	1.977
Al^{IV}	0.036	0.048	0.031	0.055	0.152	0.243	0.043	0.139	0.258	0.023
Al^{VI}	0.029	0.024	0.048	0.037	0.053	0.138	0.041	0.147	0.158	0.000
Ti	0.005	0.005	0.008	0.010	0.023	0.041	0.009	0.003	0.028	0.049
Cr	0.023	0.031	0.008	0.003	0.003	0.000	0.007	0.000	0.000	0.000
Mg	0.940	0.941	0.879	0.876	0.823	0.701	0.891	0.853	0.667	0.612
Ca	0.909	0.917	0.951	0.970	0.966	0.891	0.936	0.839	0.955	0.880
Mn	0.004	0.000	0.000	0.003	0.004	0.003	0.003	0.000	0.000	0.000
Fe^{2+}	0.072	0.069	0.083	0.096	0.149	0.232	0.098	0.152	0.213	0.372
Na	0.011	0.013	0.009	0.005	0.009	0.012	0.008	0.000	0.000	0.101
M1+M2	31.99	2.00	1.98	2.00	2.03	2.02	1.99	1.99	2.02	2.01
Mg#	93	93	91	90	85	75	90	85	76	62
Wo	45.6	45.9	47.9	48.5	47.6	44.1	47.0	42.1	47.3	43.7
En	47.1	47.1	44.3	43.8	40.6	34.7	44.7	42.8	33.0	30.4
Fs	3.6	3.4	4.2	4.8	7.4	11.5	4.9	7.6	10.5	18.5

remain valid also for CIPW normative compositions calculated for $(FeO+Fe_2O_3)$ = FeO.

Petrochemistry of the lapilli

Bulk-tuff compositions were utilized in Fig. 4A, B to illustrate their generalized variation.

Analyses were obtained by routine XRF (major and minor elements), and ICP-MS (Y, REE, Th, U) methods. Fe^{2+} was determined by redox titration; Mg by atomic absorption; CO_2 and loss on ignition (L.O.I.) gravimetrically. CO_2 values were subtracted from L.O.I. Concentrations were obtained in quadruplicate with a precision (statistical error) of better than

1% for all elements except Sc, V, Cr, Ni, Cu, Zn, Ga, and Zr, for which precision is 5% or better, respectively.

Typical bulk lapilli analyses and CIPW norms are given in Tables 7–9, sampling sites being located in Fig. 1C. Mean values from new analyses of venanzite (Table 7–8, No.11 and Table 9, No. 1) and melilitolite (Table 7–8, No.12 and Table 9, No. 2) are also given for comparison.

The bulk lapilli typically differ from venanzite in their lower (Na+K)/Al ratio, lower SiO_2-undersaturation and the presence of CIPW Or and Hy. Si, Mg, Ca, and CO_2 dominate the compositional variation, reflecting variable frac-

TABLE 3. Representative electron microprobe analyses and structural formulae of alkali feldspar from San Venanzo pyroclastic rocks. Specimen captions as in Table 1

	1 SV	2 SV	3 SV	4 SV	5 SV	6 SV
SiO_2	63.3	62.5	62.1	62.2	60.8	60.7
TiO_2	<0.01	0.12	0.08	0.13	0.14	0.09
Al_2O_3	18.8	19.1	19.2	19.5	20.3	20.5
Fe_2O_3	0.24	0.25	0.18	0.37	0.41	0.3
CaO	0.44	0.41	0.42	0.51	0.65	0.64
Na_2O	1.16	1.70	1.67	1.29	2.05	2.07
K_2O	13.9	12.5	12.5	13.0	10.8	10.6
SrO	0.58	0.62	0.73	0.77	2.05	1.99
BaO	0.79	1.64	1.35	2.09	2.26	3.1
Total	99.2	98.8	98.2	99.9	99.5	100.1

Cations based on 32 Oxygens

Si	11.835	11.742	11.731	11.656	11.477	11.427
Ti	0.000	0.017	0.011	0.018	0.020	0.013
Al	4.141	4.230	4.273	4.305	4.509	4.548
Ca	0.088	0.083	0.085	0.102	0.131	0.129
Fe^{3+}	0.051	0.053	0.038	0.078	0.087	0.066
Ba	0.058	0.121	0.100	0.153	0.167	0.232
Sr	0.063	0.068	0.080	0.084	0.224	0.217
Na	0.420	0.619	0.611	0.468	0.749	0.755
K	3.314	2.997	3.011	3.106	2.596	2.543
Total	19.97	19.93	19.94	19.97	19.94	19.93
Z	16.02	16.04	16.05	16.05	16.07	16.06
X	3.94	3.89	3.89	3.91	3.87	3.88
Or	86.7	81.0	81.2	84.5	74.7	74.2
Ab	11.0	16.7	16.5	12.7	21.5	22.0
An	2.3	2.2	2.3	2.8	3.8	3.8
Sr-fel	1.6	1.7	2.1	2.1	5.8	5.6
Ba-fel	1.5	3.1	2.6	3.9	4.3	6.0

tions of carbonate and dunite debris. Their bulk composition falls in the range of kimberlite and ultramafic rocks in terms of Cr, Co, Ni (Dawson, 1980).

Incompatible elements, normalized to a primordial mantle composition, and $[REE]_{CN}$ patterns for lapilli are shown in Fig. 3A and B, respectively, compared with patterns for venanzite and melilitolite. The lapilli patterns are very close to those for venanzite, with a slight and consistent $[REE]_{CN}$ depletion relative to venanzite. A significant $[REE]_{CN}$ and other incompatible elements enrichment for melilitolite, relative to venanzite and lapilli is apparent, Rb excepted.

The Rb depletion derives from the higher carbonate fraction in melilitolite, relative to venanzite and lapilli, which tends to enrich Ba, Sr, LREE in preference to Rb.

An average $[REE]_{CN}$ pattern for the San Venanzo carbonate (Stoppa and Woolley, 1997) is virtually parallel to those for venanzite, melilitolite and lapilli, in spite of the LREE partition coefficients strongly favourable to the carbonate at low $P-T$ (Hamilton et al., 1989). This supports the view that carbonate separation from the silicate fraction may have occurred under high $P-T$ during the rapid ascent of the CO_2-bearing primary magma.

TABLE 4. Representative electron microprobe analyses of carbonate from San Venanzo pyroclastic rocks. GM=lapilli groundmass; SEG = amoeboidal segregation in lapilli

	1 GM	2 GM	3 SEG	4 SEG	5 SEG
CaO	55.3	54.6	54.0	56.1	55.0
MgO	1.95	2.68	1.22	1.98	2.66
FeO	0.02	0.02	0.04	<0.01	0.07
MnO	0.03	0.02	0.01	<0.01	0.01
SrO	0.75	0.36	0.82	0.97	0.71
BaO	0.07	0.05	0.02	0.04	0.10
La+Ce	0.03	0.03	0.05	0.05	0.06
Total	58.15	57.76	56.16	59.16	58.61

Cations based on 6 Oxygens

	1	2	3	4	5
Ca	1.89	1.86	1.92	1.89	1.86
Mg	0.09	0.13	0.06	0.09	0.13
Sr	0.01	0.01	0.02	0.02	0.01

Petrogenesis

The silicate−carbonate system is crucial to understanding the genetic relationships between lava and pyroclastics. Irrespective of Ca occurring in carbonate or silicate phases, pyroclasts and lapilli are consistently shifted toward more silica-saturated compositions, relative to those of the lavas in the system $CaO−SiO_2−CO_2$ (Fig. 4A). Ca partitioning between CIPW larnite (Ln) and calcite (Cc), respectively (Fig. 4B), indicates that the venanzite−melilitolite transition may be related to the preferential distribution of Ca as Ln. This suggests CO_2 loss from the venanzite liquid and Ca combining with SiO_2. The compositional gap which separates the carbonatitic from other pyroclastic compositions, may reflect the experimental immiscibility reported between silicate fraction and carbonatite at less than 20 kbar (Kjarsgaard and Hamilton, 1989).

The effects of carbonatite extraction from venanzite and melilitolite liquids may be clearly visualized in terms of de La Roche's (1986)
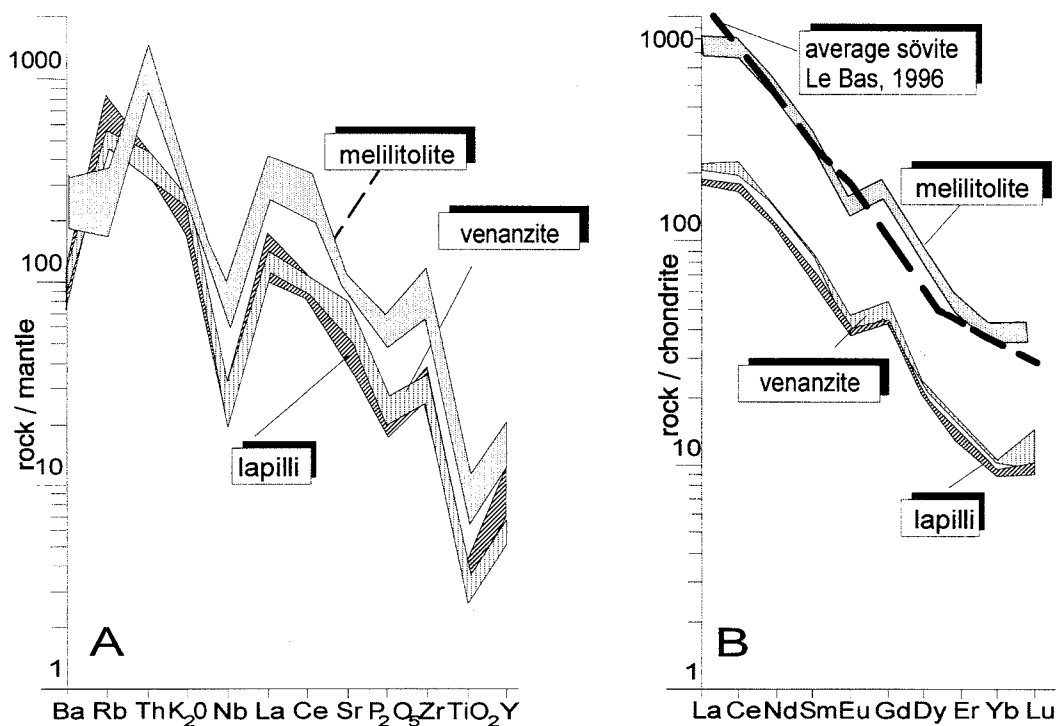

FIG. 3A, B. Multi-element diagrams of San Venanzo rocks, normalized to mantle and chondrite compositions according to Wood *et al.*, 1979; Evensen *et al.*, 1978; Nakamura, 1974. Average sövite is from data in LeBas (1996).

TABLE 5. Representative electron microprobe analyses and structural formulae of spinels from San Venanzo and Pian di Celle pyroclastic rocks. Sulphide compositions from San Venanzo pyroclastic rocks (SV 5−6) are also given. Specimen captions as in Table 1

	Spinel				Sulphides	
	1	2	3	4	5	6
	PC1	PC2	SV3	SV4	SV5	SV6
SiO_2	0.13	0.14	0.33	0.35	2.02	0.61
TiO_2	6.00	4.93	0.44	0.46	<0.01	<0.01
Al_2O_3	3.59	5.39	15.7	15.93	0.07	<0.01
Cr_2O_3	0.07	0.02	49.80	50.19	0.19	0.05
Fe_2O_3	49.62	49.50	15.70	10.71	0.00	0.00
FeO	32.21	30.87	2.50	0.62	50.00	49.60
MnO	0.83	0.67	0.52	0.18	<0.01	<0.01
MgO	2.37	2.42	14.5	14.9	0.45	0.06
CaO	<0.01	<0.01	<0.01	0.05	0.11	<0.01
NiO	<0.01	<0.01	<0.01	0.09	13.6	21.7
SO_2	<0.01	<0.01	<0.01	<0.01	27.9	22.4
Total	94.82	93.94	99.49	93.48	94.34	94.42

Cations based on 32 Oxygens

Si	0.049	0.053	0.085	0.093		
Ti	1.714	1.404	0.085	0.092		
Al	1.607	2.406	4.771	5.000		
Cr	0.021	0.006	10.153	10.569		
Fe^{3+}	14.186	14.108	3.046	2.147		
Fe^{2+}	10.235	9.778	0.540	0.139		
Mg	1.343	1.366	5.574	5.916		
Ca	0.000	0.000	0.000	0.014		
Mn	0.267	0.215	0.114	0.041		
Ni	0.00	0.00	0.00	0.019		
Total	29.42	29.34	24.37	24.03		

Ri−Rs−Rm diagram, based on cationic proportions, i.e. Ri = 2(Fe+Ti)+7(Na+K); Rs = 4(Si-Na-K); Rm = (Al+6Ca+2Mg) and given in Fig. 5A. This diagram is a chemical reduction of Yoder and Tilley's (1962) tetrahedron, suitably extended to include Fe = ($Fe^{2+}+Fe^{3+}$), Ti, and K. Differentiation trends of rock series generally tend to fan out from the [forsterite, anorthite, diopside] projection point, following curved trajectories of possible thermal lines of liquid descent toward the [nepheline, kalsilite]−[quartz] join (see de La Roche, 1986, for details). These potential differentiation trends may be modified by mineral subtraction/addition processes to silicate melts.

Carbonatite ± melilite ± forsterite ± diopside extraction from venanzite-type compositions would potentially move residual liquids toward foiditic, i.e. kalsilite-rich compositions, consistent with the Oldoinyo Lengai pyroxenite trend reported by Donaldson and Dawson (1978) and discussed by Cundari and Ferguson (1991). In the present case, this trend is delineated by venanzite/melilitolite→glass(from lapilli) (A→B; Fig. 5A). Melilitolite glass and some glass from lapilli cluster along the leucite(Lc)-sanidine(Sa) tie-line, i.e. the compositional domain of possible phonolitic residua from the differentiation of leucitite-type liquids, following the trend melilitolite→melilitolite glass (A→C; Fig. 5A). Liquids from the melilitolite, represented by cogenetic glass and falling along this tie-line may be considered as a potential source of sanidine crystallization. Liquids corresponding to the glass composition from lapilli may be also a potential source of sanidine crystallization
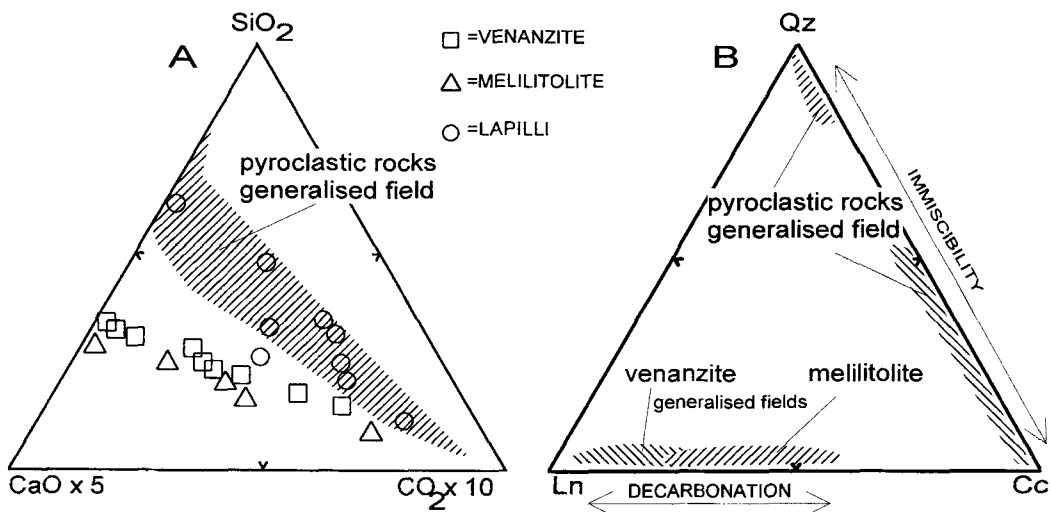
FIG. 4A. San Venanzo bulk-lapilli composition expressed in terms of SiO_2-CaO-CO_2 (wt.%). B. CIPW normative Larnite (Ln)-Ca-carbonate (Cc)-quartz(Q). Data points are from Table 7. Generalized tuff. Venanzite and melilitolite variations are from the authors' unpublished data.

along trend B→C. The green diopside, characteristic of the pyroclasts, crystallized at high Mg# values of the proposed A→C path.

Consistent with the CIPW norm (Table 7), the lapilli compositions project away from the A→B trend and cluster around the SiO_2-saturation join
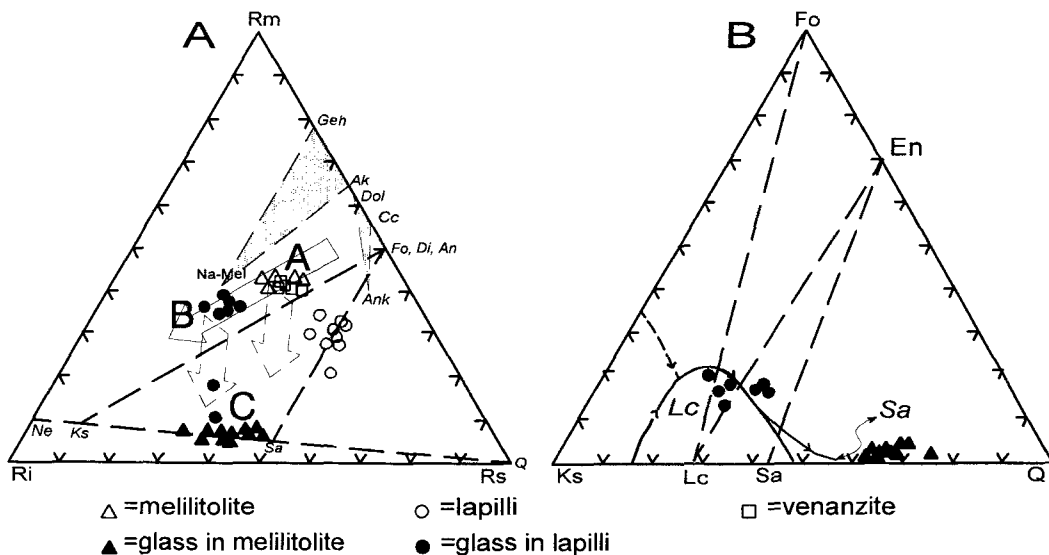

FIG. 5A. San Venanzo bulk-rock and glass compositions projected in terms of de La Roche's (1986) Ri—Rm—Rs diagram (see text). A→B: Oldoinyo Lengai pyroxenite trend (Donaldson and Dawson, 1978); A→C and B→C are potential phonolite trends (see text). B. San Venanzo glass compositions projected in the Forsterite (Fo)-Kalsilite (Ks)-Quartz (Q) system (Luth, 1967).

283

TABLE 6. Representative electron microprobe analyses and CIPW norms of glass from Pian di Celle melilitolite groundmass (MEL 1−7) and lapilli from San Venanzo pyroclastic rocks (LP 8−14). The FeO/Fe$_2$O$_3$ ratio was adjusted to 0.5, i.e. the melilitolite mean analytical value (No.12, Table 7). Mg#=Mg/(Mg+Fe^{2+}); A.I. = (Na+K)/Al; Si und (SiO$_2$ undersaturation) = negative CIPW quartz, Q

	1 MEL	2 MEL	3 MEL	4 MEL	5 MEL	6 MEL	7 MEL	8 LP	9 LP	10 LP	11 LP	12 LP	13 LP	14 LP
SiO$_2$	39.6	48.0	48.9	42.6	46.3	41.5	49.3	37.5	39.4	37.2	37.9	40.0	38.4	43.1
TiO$_2$	1.53	2.61	2.29	2.77	2.82	1.41	1.50	1.88	1.02	1.40	1.55	0.98	0.94	1.50
Al$_2$O$_3$	1.63	2.95	3.10	2.76	2.58	2.69	3.20	8.82	10.3	9.06	9.59	10.8	11.1	16.2
Fe$_2$O$_3$	7.93	6.28	6.14	5.03	6.86	7.31	0.34	3.69	2.70	2.82	3.28	2.42	2.33	4.17
FeO	15.86	12.55	12.28	10.07	13.73	14.62	0.69	7.38	5.41	5.64	6.56	4.83	4.66	8.35
MnO	0.87	0.58	0.58	0.57	0.61	0.83	0.60	0.15	0.14	0.15	0.20	0.16	0.12	0.00
MgO	0.99	1.34	1.57	1.47	1.52	0.83	1.00	6.48	7.62	6.64	6.29	6.58	5.39	9.70
CaO	2.14	2.03	1.30	1.67	1.90	2.65	1.90	16.0	13.7	15.4	14.7	15.1	17.5	0.60
Na$_2$O	3.72	5.83	6.13	6.97	3.76	5.39	6.30	1.98	1.39	1.83	1.85	1.61	1.08	0.00
K$_2$O	5.43	5.52	4.79	4.48	5.60	4.76	4.20	9.19	11.8	11.9	9.69	9.85	12.0	14.5
Total	79.70	87.69	87.07	78.39	85.68	81.99	87.13	93.07	93.48	92.04	91.61	92.33	93.51	98.12
Mg#	0.10	0.18	0.21	0.24	0.19	0.09	0.46	0.66	0.75	0.72	0.68	0.74	0.71	0.77
A.I.	8.4	5.7	5.2	6.1	5.4	5.6	4.7	1.9	2.0	2.3	1.9	1.6	1.8	1.4
K/Alk	0.6	0.5	0.4	0.4	0.6	0.5	0.4	0.8	0.9	0.9	0.8	1.0	0.9	1.0
CIPW norm														
Q	2.15	9.85	11.07	8.37	9.56	1.11	8.28							
Or	8.90	16.11	16.92	15.07	14.09	14.69	17.47							
An													1.37	
Ne									0.38					
Lc								16.38	23.42	15.31	20.93	30.32	19.95	52.53
Kp								15.49	14.98	17.01	14.58	11.11	19.98	10.63
Ac	22.95	18.16	17.76	14.57	19.85	21.15	1.00	10.68	7.82	8.16	9.49	6.99	6.73	
Ns	1.26	6.68	7.38	9.88	2.16	5.03	12.14	1.08	0.67	1.45	1.14	1.16	0.35	
Ks	6.43	4.58	3.16	3.16	5.27	3.73	2.04	1.71	3.74	5.78	1.36		2.86	
Di	9.34	8.77	5.60	7.16	8.21	11.58	7.58							
Hy	25.77	18.58	20.84	14.93	21.19	22.03								
Wo							35.79							
Ol								19.59	19.87	18.02	18.59	17.32	14.98	24.19
Cs								24.57	21.04	23.65	22.57	23.19	26.87	0.50
Mt														6.05
Ilm	2.09	4.96	4.35	5.26	5.35	2.68	2.84	3.57	1.94	2.66	2.94	1.86	1.78	2.85
Si und.								32.1	32.8	32.2	31.6	31.8	35.7	32.1

[forsterite, diopside, anorthite]-[sanidine], reflecting the contributions of mantle debris, primarily olivine, and carbonatite phases. The lapilli distribution and variation trend(s) depend on the point of separation of the carbonatitic fraction along the proposed liquid path A→C.

The system Mg$_2$SiO$_4$−KAlSiO$_4$−SiO$_2$ at or close to 1 atm (Luth, 1967) is relevant to sanidine crystallization from foidite-type liquids (Fig. 5B). Projection of representative glass compositions from lapilli in this system show that they generally cluster on the leucite (Lc) univariant line on the quartz (Q) side of the forsterite (Fo)-leucite (Lc) tie line. It is, therefore, expected that liquids corresponding to these glass compositions would crystallize leucite and sanidine under and/or close to the low-pressure volcanic regime. Melilitolite glass compositions fall within the sanidine stability field and may be considered as a potential sanidine precursor.

Model origin of the Venanzite magma

The origin and emplacement of the the San Venanzo magma, as represented by the San

TABLE 7. Representative chemical analyses and CIPW norms of lapilli from San Venanzo (SV 1−6), Celli (CEL 7) and Pian di Celle (PC 8−10) pyroclastic rocks. Sampling sites are located in Fig. 1C. Numbers refer to sample sites located in Fig. 1C. VEN11 = mean [N = 10] venanzite composition from sample sites I to X in Fig. 1C and MEL12 = mean [N = 4] melilitolite composition from sample site XI-XIV in Fig. 1C) are given for comparison. Mg# = Mg/(Mg+Fe^{2+}); A.I. = (Na+K)/Al; Si end (SiO$_2$ undersaturation) = negative CIPW quartz, Q

	1 SV/1	2 SV/2	3 SV/3	4 SV/4	5 SV/5	6 SV/6	7 CEL/7	8 PC/8	9 PC/9	10 PC/10	11 VEN	12 MEL
SiO$_2$	50.9	46.3	43.5	46.7	40.7	46.0	49.1	43.1	44.6	44.0	41.2	38.2
TiO$_2$	0.96	0.92	0.84	0.86	0.80	0.83	0.84	0.81	0.93	0.81	0.76	2.13
Al$_2$O$_3$	11.7	10.9	9.7	11.5	10.0	10.7	13.0	9.9	11.6	10.2	11.9	9.61
Fe$_2$O$_3$	6.92	4.83	4.75	4.05	4.41	3.98	4.23	5.04	4.26	3.83	3.08	3.37
FeO	2.82	3.12	2.74	3.47	2.76	3.26	3.44	1.66	3.38	3.37	3.74	6.87
MnO	0.16	0.12	0.12	0.14	0.90	0.13	0.15	0.09	0.09	0.14	0.09	0.12
MgO	11.0	14.7	15.4	13.5	13.6	15.5	12.2	7.60	11.2	10.8	11.9	9.40
CaO	2.50	4.70	7.50	5.10	10.4	5.50	5.60	13.60	8.40	9.80	15.2	17.2
Na$_2$O	0.34	0.24	0.14	0.20	0.39	0.18	0.36	0.82	0.52	0.34	0.98	1.15
K$_2$O	6.51	6.25	4.73	6.38	6.08	5.67	5.21	4.88	7.33	5.96	7.59	5.79
P$_2$O$_5$	0.45	0.41	0.40	0.37	0.41	0.36	0.36	0.33	0.43	0.40	0.47	1.21
LOI	5.23	5.70	6.27	6.01	4.36	5.47	4.97	4.51	4.13	5.13	1.43	1.81
CO$_2$	0.00	1.38	3.44	1.29	4.68	1.96	0.00	7.28	2.64	4.70	1.03	2.31
Total	99.5	99.6	99.5	99.6	99.6	99.5	99.5	99.6	99.5	99.5	99.4	99.2
Mg#	0.89	0.90	0.92	0.89	0.91	0.91	0.88	0.91	0.87	0.87	0.87	0.74
A.I.	0.91	0.93	0.79	0.89	1.01	0.85	0.67	0.80	1.05	0.96	1.12	1.11
K/(Alk)	0.95	0.96	0.97	0.97	0.94	0.97	0.94	0.85	0.93	0.95	0.89	0.83
CIPW norm												
Q	0.9											
C	0.6											
Or	38.5	36.9	28.0	37.7	26.1	33.5	30.8	28.8	33.5	35.2		
Ab	2.9	2.0	1.2	1.7		1.5	3.0	6.9		2.9		
An	9.5	10.2	11.9	11.6	7.6	11.6	18.5	8.9	7.7	8.7	5.6	4.0
Ne					1.8				2.4		4.5	5.3
Lc					7.7				7.7		35.2	26.8
Di		1.3	0.8	2.4	9.3	0.7	5.5	8.3	11.5	6.0	5.0	17.1
Hy	33.2	2.7	21.9	12.8		17.6	22.2	19.9		12.8		
Ol		20.8	15.5	18.1	25.9	18.6	8.3		20.1	12.0	21.6	15.6
Cs											16.6	11.6
Mt	6.4	7.0	6.8	5.9	6.4	5.8	6.1	3.3	6.2	5.5	4.5	5.0
Ilm	1.8	1.7	1.6	1.6	1.5	1.6	1.6	1.5	1.8	1.5	1.4	4.0
Ap	1.1	1.0	0.9	0.9	1.0	0.8	0.8	0.7	1.0	0.9	1.1	2.9
Cc	0.0	3.1	7.8	2.9	10.6	4.5	0.0	16.5	6.0	10.7	2.3	5.2
Si und.		8.5	6.3	7.4	14.1	7.6	3.3		12.2	4.8	28.2	22.1

Venanzo lava, is broadly constrained by its high anhydrous liquidus temperature of 1276°C at atmospheric pressure (Cundari and Ferguson, 1991), high Mg# and compatible element concentrations, implying a near-primary composition, and high incompatible element concentrations, pointing to small degrees of partial melting of the probable lherzolite source mantle. The associated mantle xenoliths/xenocrysts further suggest a rapid ascent, characterized by high-velocity propagation through the crust (Stoppa, 1996).

The solidus of experimental lherzolite + (H$_2$O+CO$_2$) at pressure close to 30 kbar is relevant (Wyllie, 1989; Eggler, 1989; Dalton and Wood, 1993). This shows a vapour-buffered,

TABLE 8. Representative trace element analyses of lapilli from San Venanzo (SV/1−6), Celli (CEL/7) and Pian di Celle (PC/8−10) pyroclastic rocks

	1 SV/1	2 SV/2	3 SV/3	4 SV/4	5 SV/5	6 SV/6	7 CEL/7	8 PC/8	9 PC/9	10 PC/10	11 VEN	12 MEL
Sc	nd	nd	nd	nd	22	nd	nd	nd	nd	nd	25	95
V	188	174	164	177	143	162	173	124	159	164	143	418
Cr	781	923	782	865	812	804	879	565	837	841	757	83
Co	106	39	36	47	43	39	48	45	44	36	41	40
Ni	146	158	156	157	142	152	161	109	146	145	143	37
Cu	36	36	33	34	35	30	41	36	37	33	35	43
Zn	127	99	101	102	92	99	111	90	96	97	91	94
Ga	15	16	12	13	15	13	17	12	11	16	10	19
Rb	719	532	451	471	584	455	765	451	515	495	452	224
Sr	376	397	388	515	549	460	426	1324	808	665	1720	2153
Y	60	42	42	40	38	40	55	34	48	41	29	84
Zr	424	386	379	370	331	350	396	295	384	374	345	1099
Nb	19	18	16	17	13	16	18	14	15	16	14	48
Ba	845	598	531	671	614	653	786	624	807	789	725	1935
La	123	94	90	91	67	84	98	63	97	86	85	247
Pb	23	24	27	23	26	25	13	30	29	16	28	84
Ce	212	187	171	186	149	184	193	135	210	175	189	561
Th	44	39	41	40	34	41	40	30	42	37	37	123
U	nd	nd	nd	nd	nd	nd	nd	6	nd	nd	8	24

nd = not determined

ledge-shaped configuration (Fig. 6), which marks a change from silicate to carbonatite near the solidus (White and Wyllie, 1992). Carbonate-rich melt separation from the mantle source has been experimentally demonstrated by these authors and is expected to occur rapidly at this and greater depths. It should be noted that venanzite-type melts are inconsistent with mantle $P-T$ conditions other than those prevailing at the vapour-buffered, ledge-shaped solidus (c. 1250°C and 28 kbar; Fig.6 B). These conditions may be achieved at the present lithosphere-asthenosphere transition, placed at a depth of c. 80 km under ULUD (Stoppa and Lavecchia, 1992). While a model olivine adiabat (0.8°C/km) calculated from the anhydrous venanzite liquidus is not favoured (Fig. 6B), a minimum liquidus temperature of c. 1150°C at eruption seems a reasonable hypothesis to intercept the above lherzolite ledge below the CO_2 exsolution curve.

After the initial slow ascent by percolation, magma ascent is expected to have been strongly accelerated and explosively propelled to the surface above the CO_2 exsolution boundary (Bailey, 1985; Fig. 6C). Carbonatite separation from the silicate would have occurred at less than

TABLE 9. Rare Earth Elements for mean venanzite (VEN), mean melilitolite (MEL) and lapilli. SV and PC correspond to No.5 and 8, respectively, in Table 7

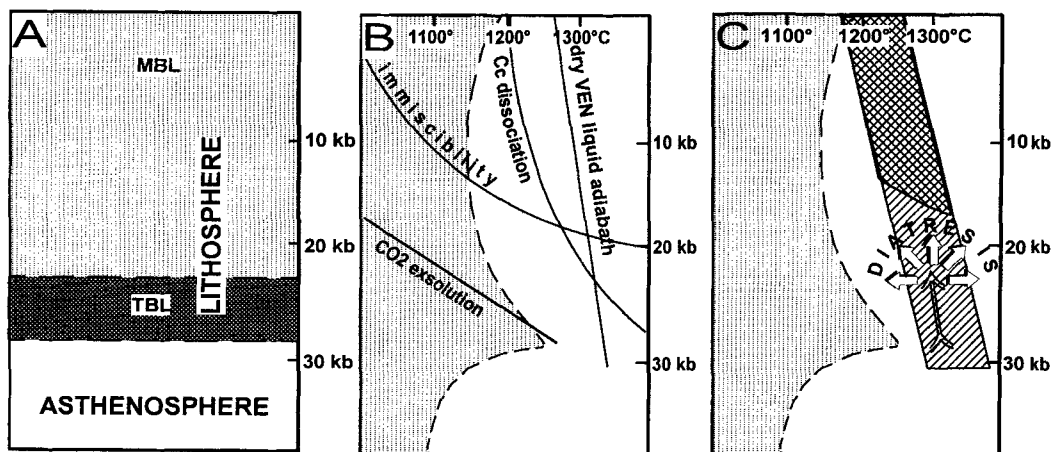|	1 VEN	2 MEL	3 SV	4 PC
La	74.27	258.80	66.40	62.70
Ce	169.50	580.50	149.00	135.00
Pr	20.30	69.60	17.50	16.80
Nd	86.55	287.00	72.50	69.60
Sm	17.00	56.20	14.70	14.20
Eu	3.07	9.93	2.83	2.75
Gd	12.50	42.85	11.70	11.30
Tb	1.50	5.30	1.35	1.30
Dy	7.53	26.75	6.51	6.60
Ho	1.19	4.01	1.05	1.03
Er	3.09	10.95	2.96	2.60
Tm	0.40	1.20	0.27	0.30
Yb	2.18	7.98	1.87	2.00
Lu	0.39	1.26	0.33	0.29
Total	399.47	1362.33	348.97	326.67

FIG. 6A. Model lithosphere structure in central Italy (Lavecchia and Stoppa, 1996), compared with B. lherzolite solidus+(CO_2, H_2O) for a model mantle composition (Wyllie, 1989; Eggler, 1989), and C. proposed origin and adiabat for the San Venanzo magma. TBL = thermal boundary layer, MBL = mechanical boundary layer.

c. 20 kbar, followed at shallow crustal levels by $CaCO_3$ dissociation and decarbonation reactions (e.g. Kjarsgaard and Hamilton, 1989; Wyllie, 1989), responsible for the unique kamafugite mineralogy. Notably, separation of the carbonatite from the silicate fraction tends to generate two independent systems which ensures the survival of carbonatite magma by escaping high-temperature, low-pressure $CaCO_3$ dissociation.

Discussion and conclusions

A close time–space relationship for effusive Ca-carbonatites and alkaline rocks containing melilite, leucite, kalsilite and perovskite is well known. Regardless of specific hypotheses for carbonatite genesis, the ubiquitous mantle debris represented by Cr-Al diopside and forsterite in the San Venanzo rocks supports the view that they derived from a mantle source (Bailey, 1993).

The $\delta^{13}C$‰ values for primary carbonates average *c.* −6 for both tuff matrix and lavas (Stoppa and Woolley, 1997; Turi, 1969). These values are compatible with mantle values and are well removed from the values obtained from the country-rock carbonate ($\delta^{13}C$‰ = 1−2; Turi, 1969). Therefore, the hypothesis that the ULUD carbonatites were generated by wall-rock carbonate assimilation (Peccerillo, 1994) cannot be supported.

Essential aspects in the genesis of the San Venanzo rock association include primarily the combination of a mantle source of unusual composition with a rapid magma ascent through the lithosphere, which involved propagation and interaction of carbonatite–venanzite liquid from its source mantle regime to the surface. The resulting magmatic system generated venanzite–carbonatite assemblages, erupted independently (e.g. Polino Ca-carbonatite) or sequentially from the same vent (e.g. Cupaello and San Venanzo). Favourable rock exposure at San Venanzo displayed their sequential relationships in the field, ranging from carbonatite-rich pyroclasts with venanzite-like lapilli to essentially silicate liquid of venanzite composition, containing subordinate carbonatite in the groundmass.

While at *P*>20 kbar venanzite-type liquids are essentially a silicate system, at and below this pressure it is expected that carbonatite separation from the silicate fraction and subsequent $CaCO_3$ dissociation set distinct but directly related evolution trends. Glass from the pyroclastic rocks reflects both carbonatite separation from the cogenetic silicate fraction and possible derivation from a phonolitic liquid at the very top of the magmatic column. This liquid would have been dissipated as volcanic ash by the initial, violent activity of the San Venanzo volcanoes, which preserved sanidine crystals, concentrated in the early tuff layers, and green diopside, crystallized from higher Mg# variants of the same liquid.

The rare and extreme composition of the San Venanzo rocks implies low mantle melting

degrees and rapid melt separation and ascent to the surface. These constraints are related to incipient thinning of continental lithosphere during rift propagation, consistent with the observed tectonic regime associated with ULUD rocks in Italy and elsewhere.

Acknowledgements

References

Bailey, D.K. (1993) Carbonate magmas. *J. Geol. Soc. London*, **150**, 637–51.

Bailey, D.K. (1985) Fluids, melts, flowage and styles of eruption in alkaline–ultra-alkaline magmatism. *Trans. Geol. Soc. S. Afr.*, **88**, 449–57.

Bailey, D.K. (1990) Mantle carbonatite eruptions: Crustal context and implications. *Lithos*, **26**, 37–42.

Bell, K. and Powell, J.L. (1969) Strontium isotopic studies of alkalic rocks: the potassium-rich lavas of Birunga and Toro-Ankole regions, east and central equatorial Africa. *J. Petrol.*, **10**, 536–72.

Brozzetti, F. and Stoppa, F. (1995) Le Piroclastiti medio-pleistoceniche di Massa-martana-Acquasparta (Umbria): caratteri strutturali e vulcanologici. *Il Quaternario*, **8**, 95–110.

Clark, L.A. and Kullerud, G. (1959) The Fe–Ni–S system: the phase relations between pyrite and vaesite in presence excess of sulphur. *Carnegie Inst. Washington Ann. Rep. Dip. Geophys. Lab.*, **57**, 229.

Cundari, A. and Ferguson, A.K. (1982) Significance of the pyroxene chemistry from leucite-bearing and related assemblages. *Tschermaks Mineral. Petrogr. Mitt.*, **30**, 189–204.

Cundari, A. and Ferguson, A.K. (1991) The Roman Comagmatic Region: The lavas of S. Venanzo and Cupaello. *Contrib. Mineral. Petrol.*, **107**, 343–57.

Dalton, J.A. and Wood, B.J. (1993) The composition of primary carbonate melts and their evolution through wallrock reaction in the mantle. *Earth Planet Sci. Lett.*, **119**, 511–25.

Dawson, J.B. (1980) Kimberlites and their xenoliths. *Minerals and Rocks*, **Vol. 15**, Spinger Verlag, New York, pp 252.

de Albuquerque Sgarbi, P.B. and Gomes-Valença, J. (1993) Kalsilite in Brazilian kamafugitic rocks. *Mineral. Mag.*, **57**, 165–71.

de La Roche, H. (1986) Classification et nomenclature des roches ignées: un essai de restauration de la convergence entre systèmatique quantitative typologie d'usage et modèlisation gènètique. *Bull. Soc. Geol. Fr.*, **2**, 337–53.

Donaldson, C.H. and Dawson, J.B. (1978) Skeletal crystallization and residual glass composition in a cellular alkalic pyroxenite nodule from Oldoinyo Lengai. *Contrib. Mineral. Petrol.*, **67**, 139–49.

Eggler, D.H. (1989) Carbonatites primary melts and mantle dynamics. In *Carbonatites: Genesis and Evolution*, (K. Bell, ed.), Unwin Hyman, London, pp 561–79.

Evensen, M.M., Hamilton, P.J. and O'Nions, R.K. (1978) Rare-Earth abundance in chondritic meteorites. *Geochim. Cosmochim. Acta*, **42**, 1199–212.

Foley, S.F., Venturelli, G., Green, D.H. and Toscani, L. (1987) The ultrapotassic rocks: characteristics classification and constrains for petrogenetic models. *Earth Sci. Rev.*, **24**, 81–134.

Gallo, F., Giammetti, F., Venturelli, G. and Vernia, L. (1984) The kamafugitic rocks of San Venanzo and Cupaello, central Italy. *Neues Jahrb. Mineral., Mh.*, 198–210.

Hamilton, D.L., Bedson, P. and Esson, J. (1989) The behaviour of trace elements in the evolution of carbonatites. In *Carbonatites: Genesis and Evolution*, (K. Bell, ed.), Unwin Hyman Ltd London, pp 405–27.

Holmes, A. (1942) A heteromorph of Venanzite. *Geol. Mag.*, **79**, 225–32.

Kapustin, Y.L. (1980) *Mineralogy of Carbonatites*. Amerind Publishing Co. Pvt. New Delhi, pp 259.

Kjarsgaard, B.A. and Hamilton, D.L. (1989) The genesis of carbonatites by immiscibility. In *Carbonatites: Genesis and Evolution*, (K. Bell, ed.), Unwin Hyman Ltd London, pp 388–404.

Lavecchia, G. and Stoppa, F. (1996) The tectonic significance of Italian magmatism: an alternative view to the popular interpretation. *Terra Nova*, **8**, 435–46.

Lavecchia, G., Brozzetti, F., Barchi, M., Menichetti, M. and Keller, J.A. (1994) Seismotectonic zoning in east-central Italy deduced from an analysis of the Neogene to present deformations and related stress field. *Geol. Soc. Amer. Bull.*, **106/9**, 1107–200.

LeBas, M.J. (1987) Nephelinites and carbonatites. In *Alkaline Igneous Rocks* (J.G. Fitton and B.G.J. Upton, eds), Vol. **30**, Geol. Soc. Spec. Publ., 53–83.

LeBas, M.J. (1996) Standard rare earth element composition for sovitic and alvikitic carbonatites. In *Geochemical Studies on Synthetic and Natural Rock Systems*, (A.K. Gupta, K. Onuma and M Arima, eds.), (Kenzo Yagi volume). Allied Press, New Delhi, 90–110.

LeMaitre, R.W., Batema, P., Dudek, A., Keller, J., Lameyre, J., LeBas, M.J., Sabine, P.A., Schmid, R.,

Sørensen, H., Streckeisen, A., Woolley, A.R. and Zanettin, B. (1989) *A classification of Igneous Rocks and Glossary of Terms*. Blackwell, Oxford, pp 193.

Luth, W.C. (1967) Studies in the system $KAlSiO_4$–$MgSiO_4$–SiO_2–H_2O: I. Inferred phase relations and petrologic applications. *J. Petrol.*, **8**, 372–416.

Mitchell, R.H. (1986) *Kimberlites: Mineralogy, Geochemistry and Petrology*. Plenum Press, New York, pp 442.

Mitchell, R.H. (1995) *Kimberlites, Orangeites, and Related rocks*. Plenum Press, New York, pp 410.

Mitchell, R.H. and Bergman, S.C. (1991) *Petrology of Lamproites*. Plenum Press, New York, pp 447.

Mittempergher, M. (1965) Volcanism and petrogenesis in the San Venanzo area (Italy). *Bull. Volccanol.*, **28**, 85–94.

Moore, A.E. and Erlank, A.J. (1985) Unusual new olivine zoning: evidence for complex physico-chemical changes during the evolution of olivine melilitite and kimberlite magmas. *Contrib. Mineral. Petrol.*, **70**, 391–405.

Morimoto, N. (1988) Nomenclature of pyroxenes. *Mineral. Mag.*, **52**, 535–50.

Nakamura, N. (1974) Determination of *REE* Ba Fe Mg Na and K in carbonaceous and ordinary chondrites. *Geochim. Cosmochim. Acta*, **38**, 757–75.

Peccerillo, A. (1994) Mafic ultrapotassic magmas in central Italy: geochemical and petrological evidence against primary copositions. *Miner. Petrogr. Acta*, **37**, 229–45.

Peccerillo, A., Poli, G. and Serri, G. (1988) Petrogenesis of orenditic and kamafugitic rocks from central Italy. *Canad. Mineral.*, **26**, 45–65.

Rosenbusch, H. (1898) Uber Euktolith ein neues Glied der theralithischen Effusivmagmen. *Sitzungberichte der K. Preussischen Akad.*, **7**, 110.

Sabatini, V. (1899) I vulcani di San Venanzo. *Riv. Ital. di Min. Cristallogr.*, **22**, 3–12.

Sahama, T.G. (1974) Potassium-rich alkaline rocks. In: H. Sörensen, ed, *The Alkaline Rocks*, Wiley, New York, pp 622.

Smith, J.V. and Brown, W.L. (1989) *Feldspar Minerals II*, Springer-Verlag, Heidelberg.

Stoppa, F. (1996) The San Venanzo maar and tuff-ring Umbria Italy: eruptive behaviour of a carbonatite-melilitite volcano. *Bull. Volcanol.*, **57**, 563–77.

Stoppa, F. and Cundari, A. (1995) A new Italian carbonatite occurence at Cupaello (Rieti) and its genetic significance. *Contrib. Mineral. Petrol.*, **122**, 275–88.

Stoppa, F. and Lavecchia, G. (1992) Late-Pleistocene ultra-alkaline magmatic activity in the Umbria-Latium region (Italy): An overview. *J. Volcanol. Geotherm. Res.*, **52**, 277–93.

Stoppa, F. and Lupini, L. (1993) Mineralogy and petrology of the Polino monticellite-Ca-carbonatite central Italy. *Mineral. Petrol.*, **49**, 213–32.

Stoppa, F. and Sforna, F. (1995) Geological map of the San Venanzo volcano (Central Italy): Explanatory notes. *Acta Volcanol.*, **7**, 85–91.

Stoppa, F. and Woolley, A.R. (1997) Italian carbonatites: field occurrence petrology and regional significance. *Mineral. Petrol.*, **59**, 43–67.

Stoppa, F., Sharygin, V. and Cundari, A. (1997) New mineral data from the kamafugite-carbonatite association:-the melilitolite from San Venanzo, Italy. *Mineral. Petrol.*, **78/3–4**, 251–65.

Turi, B. (1969) Composizione isotopica dell'ossigeno e del carbonio dei carbonati presenti nelle vulcaniti di San Venanzo (Umbria). *Period. Mineral.*, **38**, 589–603.

White, B.S. and Wyllie, P.J. (1992) Solidus reactions in synthetic lherzolite-H_2O-CO_2 from 20–30 kbar with applications to melting and metasomatism. *J. Volcanol. Geotherm. Res.*, **50**, 117–30.

Wood, D.A., Joron, J. and Treuil, M. (1979) A re-appraisal of the use of trace elements to classify and discriminate between magma series erupted in different tectonic settings. *Earth Planet. Sci. Lett.*, **45**, 326–36.

Wyllie, P.J. (1989) Origin of carbonatites: evidence from phase equilibrium studies. In *Carbonatites: Genesis and Evolution*, K. Bell, ed, Unwin Hyman, London, pp 500–45.

Yoder, H.S. Jr and Tilley, C.E. (1962) Origin of basaltic magmas: An experimental study of natural and synthetic rock systems. *J. Petrol.*, **3**, 342–532.